Oligocellulose from acid hydrolysis: A revisit

Feng Jiang, Xin Zhang, Wonseok Hwang, Yoshiharu Nishiyama, Robert Briber, Howard Wang

Oligocellulose from Acid Hydrolysis: A Revisit

Feng Jiang[a,b,#], Xin Zhang[b,#], Wonseok Hwang[c], Yoshiharu Nishiyama[d], Robert M. Briber[b,*], Howard Wang[b,e,*]

[a] Biomass Molecular Engineering Center, Department of Materials Science and Engineering, School of Forestry and Landscape Architecture, Anhui Agricultural University, Hefei, Anhui 230036, China

[b] Department of Materials Science and Engineering, University of Maryland, College Park, Maryland 20742, United States

[c] Department of Chemistry and Biochemistry, University of Maryland, College Park, Maryland 20742, United States

[d] Cermav, CNRS, Grenoble, France

[e] Neutron Science Platform, Songshan Lake Materials Laboratory, Dongguan, Guangdong 523808, China

[#] These authors contributed equally to this work

ABSTRACT

The classical method of producing cellulose oligomers through hydrolysis of microcrystalline cellulose (MCC) in phosphoric acid has been re-examined. Hydrolysis products are fractionated by precipitation to yield two types of cellulose oligomers with different average degrees of polymerization (DP). The number- and weight-averaged molecular weights of the lower DP fraction are 1339 g/mol and 1388 g/mol respectively corresponding to a polydispersity index of 1.04. The cellulose oligomer forms type-II crystal, and can be dissolved in both alkaline aqueous solutions and dimethyl sulfoxide. The X-ray and neutron small angle scattering of the cellulose oligomers in solution can be described as rigid slabs.

Key words: Oligomeric cellulose; acid hydrolysis; polymer physics; small angle neutron scattering

1. Introduction

Cellulose is the most abundant biomacromolecule on the planet Earth, in which β-1,4-linked anhydroglucose units (AGU) form long chains that are organized into crystalline nanofibrils [1, 2]. Cellulose has found uses in many aspects of everyday life throughout human history, and potential applications in modern technologies [3-7]. However, limited by poor processability at the molecular level, the full potential of the renewable biomacromolecules is underutilized. Low molecular mass oligomeric cellulose (OC) can be used as model molecules for a better understanding of the chemical and physical nature of cellulose and its derivatives [8], in addition to finding immediate applications in biomedical and food industries [9, 10]. An easy-to-implement, well-characterized process for cellulose oligomer production is essential for advancing the science and technology of biomacromolecules in general and cellulose in particular.

Various methods have been developed to produce OC, including chemical [11] and enzymatic synthesis [12], alkaline [13] and enzymatic degradation [14], acetolysis and deacetylation [15], and acid hydrolysis [16]. For scalable productions, enzymatic depolymerization and acid hydrolysis are considered the more viable methods, with the former potentially useful for the industrial-scale production of water-soluble glucose, cellobiose or cellotetraose as chemical energy sources, and the latter suitable for producing cellulose oligomers with variable degree of polymerization (DP) and polydispersity depending on specific acids and hydrolysis conditions. Hydrolyses in hydrochloric,

sulfuric and nitric acids are often affected by side-reactions to form foreign molecules, resulting in low purity and low yield of cellulose oligomer products [17-19], while phosphoric acid (H_3PO_4) hydrolyzes cellulose effectively and has lower volatility and toxicity compared to other strong acids. Upon immersing in concentrated H_3PO_4, crystalline cellulose fibers dissolve to form a homogeneous solution; subsequently, cellulose chains undergo a three-step hydrolysis process: (1) protonation of the glycosidic oxygen, (2) formation of pyranosyl cations, and (3) addition/heterolytic cleavage of water molecules [8].

In a seminal study, Isogai and coworkers have demonstrated H_3PO_4-hydrolysis production of two OC fractions with DP peaked at 7 and 15, denoted as DP7 and DP15, respectively [20]. In that original work, the molecular weight distributions were obtained indirectly through intrinsic viscosity and high-performance size-exclusion chromatography (HPSEC) measurements on cellulose tricarbanilate derivatives. In this study, we have revisited the H_3PO_4-hydrolysis method and characterized the molecular characteristics of neat OC products using a collection of modern instruments, including matrix-assisted laser desorption/ionization time-of-flight mass spectrometer (MALDI-TOF MS), Fourier-transform infrared (FTIR) spectroscopy, nuclear magnetic resonance (NMR) spectroscopy, wide angle X-ray scattering or diffraction (WAXS, XRD), scanning electron microscopy coupled with energy dispersive X-ray (SEM-EDX) analysis,, small angle X-ray and neutron scattering (SAXS and SANS). Due to the higher molecular

weight, DP15 shows poor solubility in common solvents. The preparation of DP7 is fully repeatable, and DP7 can be well dissolved in DMSO, enabling the preparation of cellulose crystals and cellulose derivatives. Therefore, we are mainly focused on DP7 in this work. We obtained a quantitative depiction of the DP7 and confirmed the previous findings, and also revealed the existence of cellulose phosphate in the cellulose oligomer products.

2. Experimental section

2.1. Materials

Microcrystalline cellulose (MCC, Avicel PH-101), phosphoric acid (85 % by mass aqueous solution), sodium hydroxide (NaOH), lithium hydroxide (LiOH), hydrochloric acid (HCl) and acetone were purchased from Sigma-Aldrich, deuterated dimethyl sulfoxide (dDMSO) and deuterium oxide were obtained from Cambridge Isotopes. They were used as received. Following the reported method [20] with slight modifications, 24.0 g MCC was mixed with 18 mL deionized water in a 500 mL glass bottle, and then 85% H_3PO_4 (450 mL) was introduced. A clear solution formed after about 8 days at room temperature without stirring. After 9 weeks, the dark brown solution was precipitated into 5 L deionized water and filtered after 2 hours. The precipitates were collected and denoted as DP15. The filtrate was added into 6 L methanol and stored overnight. A white precipitate was collected by centrifugation and washed thoroughly with deionized water and acetone, and denoted as DP7. Upon drying the solids under vacuum at room

temperature, the overall yield of cellulose oligomer products from the two precipitates was found at ca. 50% by mass of the starting MCC, in which the range of yield for DP7 is 12-20 %, and for DP15 at 25-50 %, respectively.

2.2. Characterization

FTIR spectra of pristine MCC, regenerated cellulose from alkaline solution of MCC, and DP7 were recorded on Nicolet Nexus 670 FTIR spectrometer with an attenuated total reflectance (ATR) with a single reflection diamond plate. Regenerated cellulose was prepared by dissolving MCC in 12 wt % NaOH aqueous solution at -15 ºC, precipitating in 0.4 wt % HCl, followed by continuous water rinse to a neutral pH. NMR measurements were carried out using a Bruker Avance 400 NMR spectrometer on 1 wt % solution in dDMSO. MALDI-TOF MS spectra were obtained with a Bruker Autoflex Speed spectrometer using 2,5-dihydroxybenzoic acid (DHB) as the matrix in both positive- and negative-ion modes. EDX spectra were collected on a Hitachi SU-70 Field Emission SEM using a Bruker EDX detector. WAXS and SAXS data were recorded using a Xenocs Xeuss instrument with a micro-focus source of the copper Kα radiation (λ = 1.5418 Å). SAXS measurements were done on 1-5 wt % DP7 dissolved in 4 wt % LiOH aqueous solutions loaded in a 1 mm diameter capillary with 10 µm wall thickness. SAXS data were reduced by subtracting the data from solvent in capillary as background after normalization with the transmission and exposure time. SANS on 1 wt % DP7 in dDMSO were carried out on the NGB-30 m SANS at the NIST Center for Neutron Research (NCNR), National Institute of

Standards and Technology (NIST). The neutron wavelength λ = 6 Å with a spread $\Delta\lambda/\lambda$ of 12%. The scattering was measured over a *Q*-range from ~0.003 Å^{-1} to ~0.5 Å^{-1}, where Q is the momentum transfer, $Q = \left(\frac{4\pi}{\lambda}\right)\sin(\frac{\theta}{2})$, with θ being the scattering angle. Data reduction were carried out using the IGOR Pro macros by subtracting blocked beam background, correcting detector efficiency, converting to absolute scattering cross-section, and averaging 2D data into 1D spectra, *I(Q)*.

3. Results and discussion

3.1. Chemical and crystal structures of OC

FTIR spectra of MCC, RC and DP7 are shown in Fig. 1. Well-established spectral characteristics can be identified from the MCC spectrum, in which bands in the range from 3700 to 2995 cm^{-1} are attributed to hydrogen-bonded OH stretching. The bands at 2896 cm^{-1}, 1641 cm^{-1}, and 1428 cm^{-1} are assigned to CH stretching vibrations, OH bending vibrations of adsorbed water, and CH_2 scissoring motion, respectively. The C-H deformation vibration and C-O stretching vibration can be found at 1367 cm^{-1} and 1029 cm^{-1}, respectively. The band at 897 cm^{-1} is attributed to the anomeric C1-H ring valence vibration [21]. The DP7 shows a broader hydrogen-bonded OH stretching band around 3336 cm^{-1} and stronger 897 cm^{-1} peak, due to the rearrangement of hydrogen bonding and reorientation of hydroxymethyl group in oligocellulose. The infrared spectra of DP7 is almost identical to that of RC and is typical of cellulose II allomorph [22], consistent with literature [23-26].

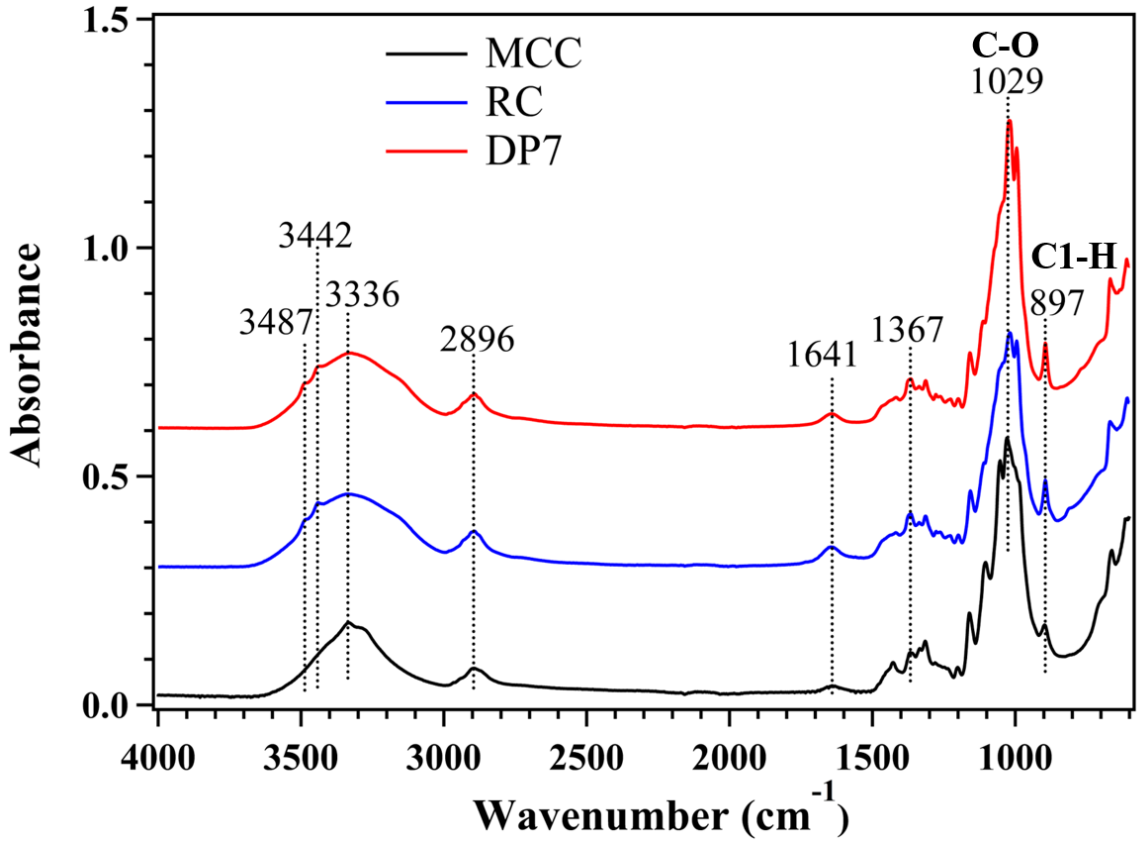

Fig. 1. FTIR spectra of microcrystalline cellulose (MCC), regenerated cellulose (RC), and oligocellulose DP7 in the regime of 4000-600 cm^{-1}. The absorbance was normalized to CH stretching at 2896 cm^{-1}. The spectra of RC and DP7 are shifted upward for clarity.

Thoroughly washed and dried DP7 powders as shown in Fig. S1 in the Supplementary Information have been measured using X-ray diffraction. As shown in Fig. 2, WAXD pattern of DP7 shows strong diffraction peaks at 2θ angles of 12.2º, 20.0º, and 22.1º, which, according to calculated XRD spectrum using Mercury software from the Cambridge

Crystallographic Data Center (CCDC) based on the cellulose II structure shown in the inset of Fig. 2, correspond to ($1\bar{1}0$), (110) and (020) crystallographic planes [27, 28].

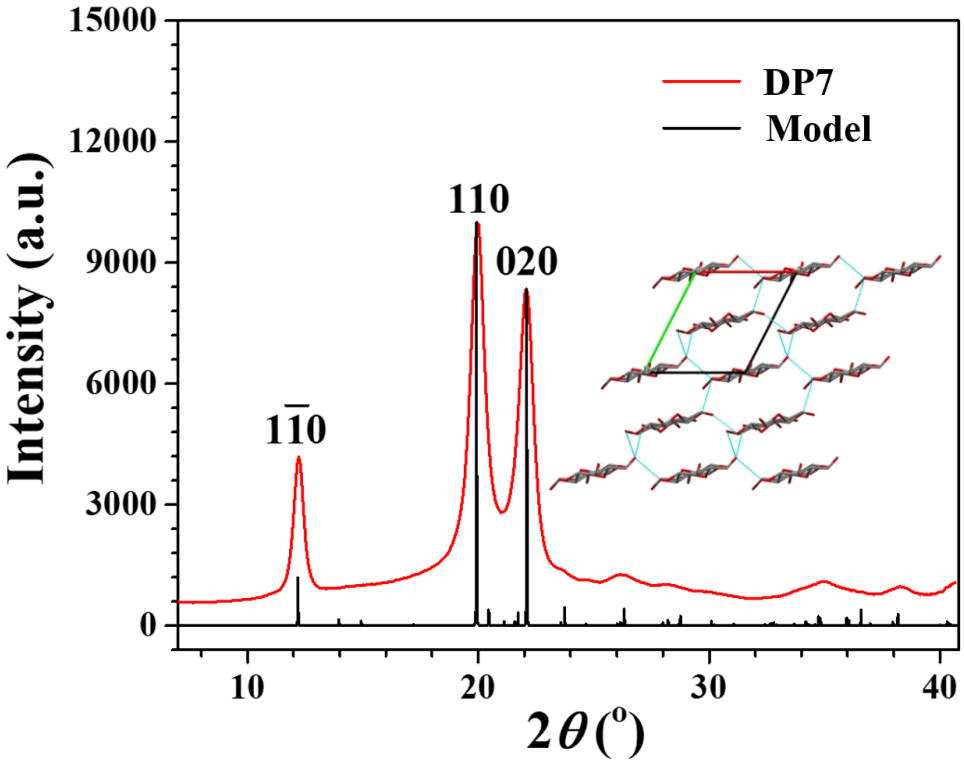

Fig. 2. The X-ray diffraction pattern of DP7 show prominent diffraction peaks of ($1\bar{1}0$), (110) and (020) crystallographic planes. Computed X-ray diffraction patterns of type-II cellulose crystal structure convoluted with 0.01° FWHM is also shown. Inset is the illustration of cellulose II crystal structure viewing from the c direction.

The ^{1}H and ^{13}C NMR spectra of DP7 in dDMSO are shown in Fig. 3 and Fig. S2, respectively. The chemical shifts are identified and annotated on the chemical structure of cellulose on the basis of previous studies [29-32]. As displayed in Fig. 3, the peaks in the 4.9-2.8 ppm region are ascribed to the CH and CH_2 protons of the AGU. The weak peaks at

4.85 and 4.37 ppm are attributed to the α- and β-anomeric protons at the reducing end of oligocellulose. The peaks in 6.7-4.4 ppm can be ascribed to the protons of hydroxyl groups. Furthermore, the chemical shifts at 6.30 and 6.64 ppm are due to the hydroxyl protons of α- and β-anomers at reducing ends of cellulose. Given the quantitative measurements of ^{1}H resonance intensity from specific locations on chain ends and all AGU's, the number averaged DP can be calculated as follows [33]

$$DPn = \frac{I_\alpha + I_\beta + I_1}{I_\alpha + I_\beta} = 1 + \frac{I_1/I_\alpha}{1 + I_\beta/I_\alpha} \qquad (1)$$

where I_α and I_β are the integrated intensities of each peak in (α-H1, β-H1) and (α-OH1, β-OH1) couples, and I_1 from the H1′,1″. The averaged I_β/I_α = 1.10 and I_1/I_α = 13.9, resulting in DP~7.6, consistent with the previous study [20].

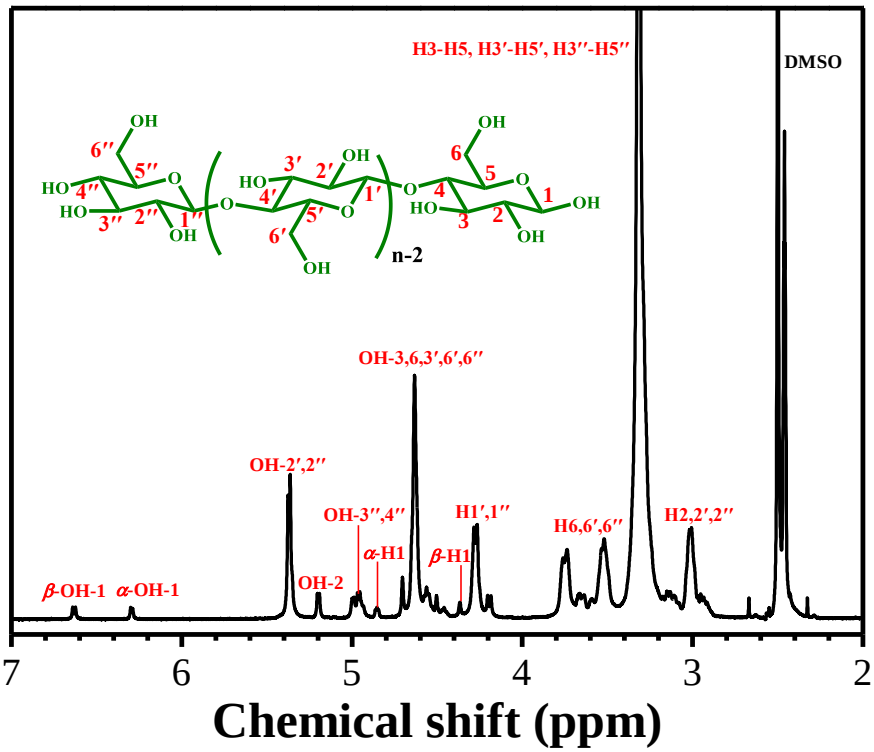

Fig. 3. ^{1}H NMR spectrum of DP7 in dDMSO. Characteristic chemical shifts corresponding to specific bonds are annotated on the chemical structure of the cellulose molecule in the inset.

3.2. Molecular mass and polydispersity index (PDI) of OC

The MALDI-TOF MS spectrum of counts as a function of mass-to-charge (*m/z*) ratio in the positive-ion mode is shown in Fig. 4a. Well resolved spectral lines with sub-atomic-unit resolution imply both high purity OC and high-fidelity measurements. The adjacent main lines are separated by *m/z* = 162, corresponding to one AGU repeating unit. The primary lines correspond to the sum of the mass of one cellulose molecule containing ^{12}C for all carbon atoms and one Na ion, which is acquired in the process of ionization, while satellite lines separated by one atomic unit to the right of the mainline, as shown in Fig. 4b and c for DP7 and DP11, respectively, corresponding to the inclusion of 1-3 ^{13}C atoms in individual oligocellulose molecules. The distribution profiles of ^{13}C have been examined by comparing the MALDI data with the theoretical prediction according to the random distribution of carbon isotopes, as shown in Fig. 4d, in which the vertical axis is the ratio of the abundance of oligocellulose molecules containing 1-3 ^{13}C to that of the corresponding neat ^{12}C ones. The diagonal line represents an average ^{13}C abundance of 1.084 ± 0.008 % in the specimen, lower than the overall natural abundance of 1.109%. The percentage histogram of different DPs as color-coded species containing 0-3 ^{13}C for each DP is shown in Fig. 4e. Data display the dominance of DP7 and DP8 oligocellulose,

and the polydispersity of the specimen spanning over the range of 5-12 AGU. The number- and weight-averaged molecular weight (M_n and M_w) and PDI value are calculated through a simple summation of all species [34], yielding M_n = 1339 g/mol, M_w = 1388 g/mol, and PDI = 1.04, respectively. The corresponding number-averaged DP value is 8.15. The narrow distribution of DP7 is a result of dual precipitations, in water to remove the high DP fraction, and in methanol with water and acetone wash to remove the low DP species and other impurities [16].

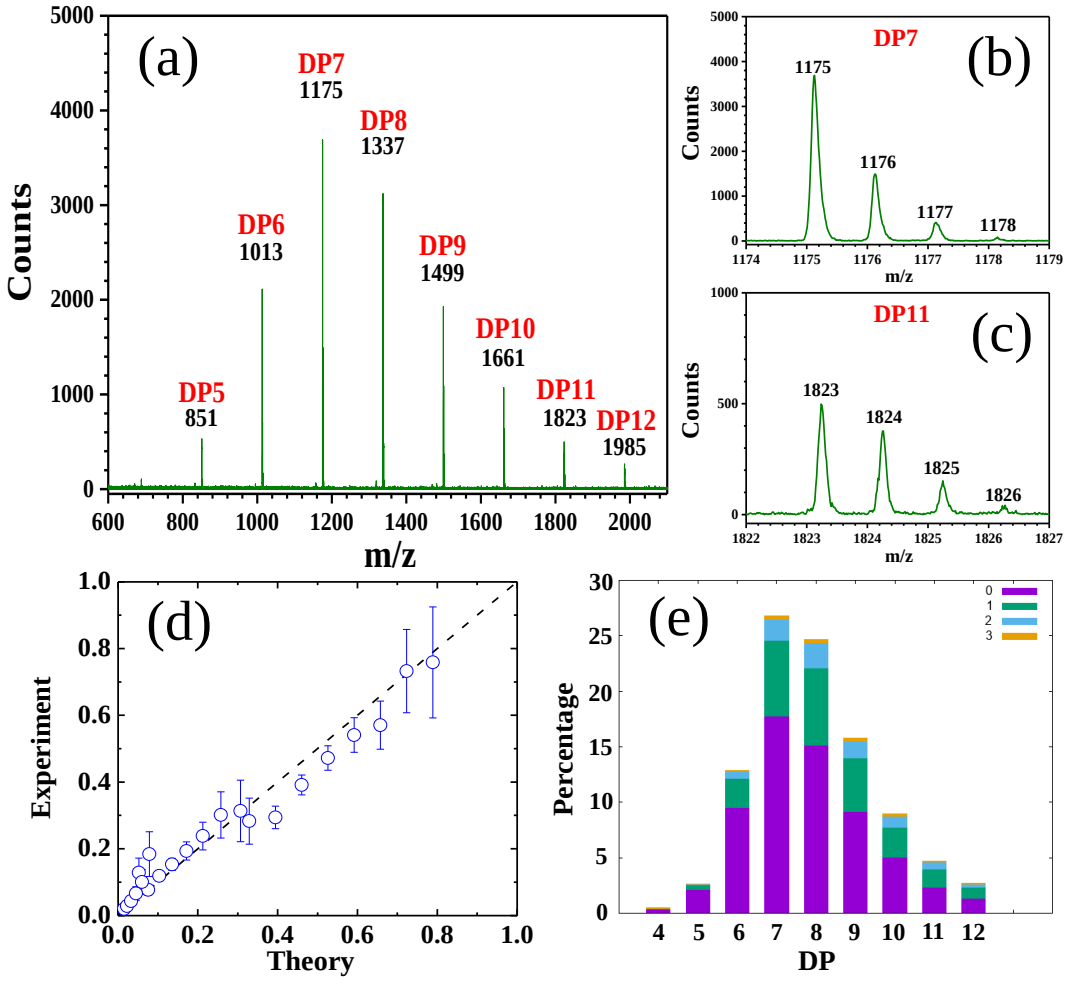

Fig. 4. (a) Positive-ion mode MALDI counts as a function of mass-to-charge (*m/z*) ratio for the oligocellulose DP7. The molecular mass quantity and corresponding DPs are marked on top of each mainline. The DP has a range of 5-12 and peaks at 7. The details of spectrum at DP7 (b) and DP11 (c) show satellite peaks with consecutive addition of 1-3 atomic mass number. (d) The ratio of peak areas of ^{13}C-containing species to their primary neat-^{12}C peak compared with the prediction based on the random distribution probability. (e) Percentage histogram of different-DP oligocellulose with color-coding for 0 (purple), 1 (green), 2 (blue) and 3 (orange) ^{13}C in one cellulose molecule, respectively.

MALDI-TOF MS spectrum in negative-ion mode was slightly different, as shown in Fig. 5. The lines are separated by the AGU mass of 162, with the mainline quantity equaling to the sum of the mass of one cellulose molecule and one phosphoryl group PO_3^- (mass value of 79). The DP of cellulose was in the range of 7-15 and peaked at 9, apparently higher than those measured in positive-ion mode. It is conceivable that the measured molecules are cellulose phosphate, which are formed via a C-O-P bond during hydrolysis, and lose one proton and become negatively charged during ionization. Because of the higher solubility of cellulose phosphate in water and protic solvents, it is expected that dual-precipitation and wash process result in an overall higher DP of cellulose phosphate.

It is desirable to quantify the amount of phosphorus in cellulose oligomer product DP7. The very high noise level of the MALDI-TOF MS spectrum in negative-ion mode implies

low population of cellulose phosphate. The FTIR spectra shown in Fig. 1 does not detect the existence of phosphorus. EDX measurements yield semi-quantitative assessment of phosphorus by revealing ca. 0.13 *at*% of phosphorus in the specimen (Fig. S3). Because of the higher sensitivity of EDX to heavier element phosphorus, and the possibility of electron beam damage to the specimen by selectively vaporizing volatile organic moieties while leaving the phosphorus behind, EDX date do not yield a quantitative measure of the phosphorus composition [35]. The phosphorylation during acid-hydrolysis has not been previously reported, the mechanism and location of phosphate bond remain uncertain, further studies are needed.

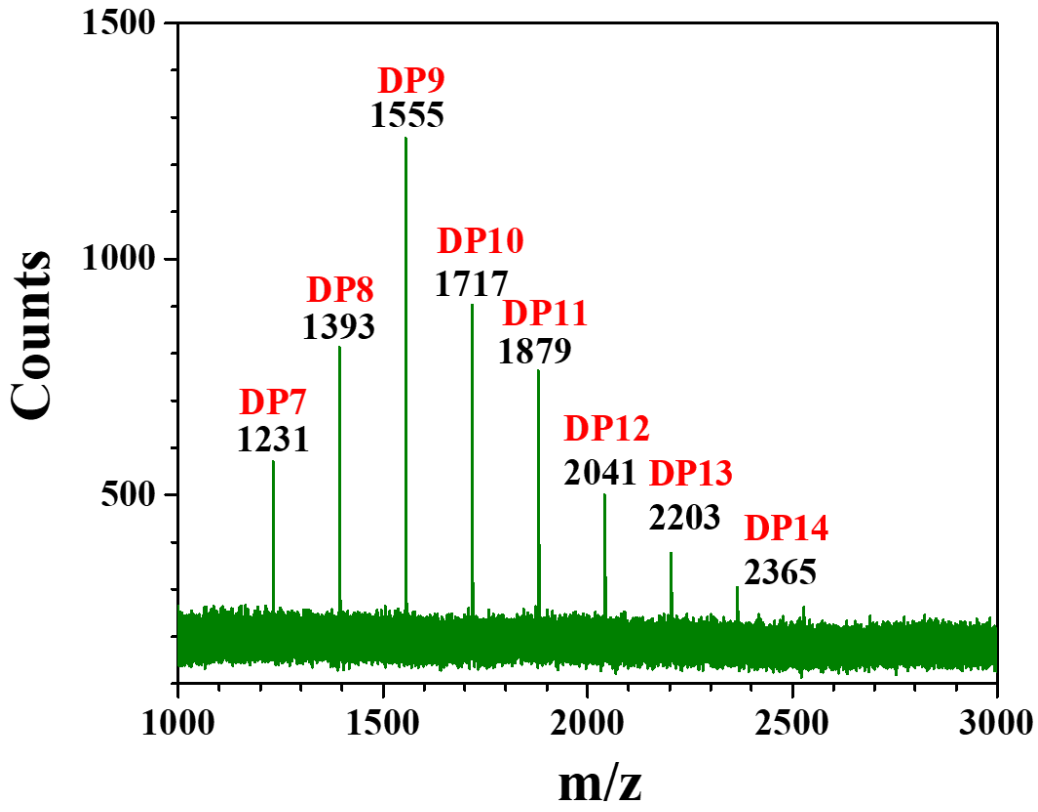

Fig. 5. Negative-ion mode MALDI-TOF MS spectrum of the oligocellulose DP7. The molecular mass quantity and corresponding DPs are marked on top of each mainline. The DP has a range of 7-15 and peaks at 9. Note the very high noise level for measuring negative ion species.

3.3. SAXS and SANS analysis

SAXS and SANS patterns of 1, 2 and 5 wt % of DP7 in 4 wt % of LiOH aqueous solutions, as well as 1 wt % DP7 in dDMSO are shown in Fig. 6. The plateau at low-Q region implies cellulose oligomer solutions without aggregation in both alkaline and organic solvents. A medium-Q region with a power-law of Q^{-1} indicates 1D-like structure, i.e. extended conformation of DP7 in alkaline solution, followed by a transient Q^{-2} scaling in the high-Q region due to the flat shape of glucose residue. The radius of gyration (R_g) of dispersed particles is analyzed from the low-Q region of small angle scattering using Guinier law, $I(Q) = I_0 exp\left(-Q^2 R_g^2/3\right)$, where I_0 is the zero angle scattering at Q = 0. Linearized plot with fitting as shown in the inset of Fig. 6 yields R_g = 10.2 ± 0.3 Å for the 5 wt % DP7. Same analyses have been applied to 1 and 2 wt % solutions to yield R_g's at 10.5 ± 0.4 Å and 11.0 ± 0.6 Å, respectively. Due to deprotonation of the hydroxyl groups to afford charged side chains at high pH [36] and the intrinsically rigid backbones, cellulose oligomers can be assumed to take rigid rod-like conformation. Using a model of cylindrical rod with a radius R = 3 Å, the average length of DP7 is estimated from R_g with equation,

$L^2 = 12R_g^2 - 6R^2$, yielding L = 36 Å. Given the length of AGU at 5.15 Å [37-40], the average DP ~ 7 is consistent with the NMR and MALDI-TOF MS results.

The scattering curves over the entire *Q*-range were also fitted with a parallelepiped model using SASView 5.0; the best fitting curves are plotted on the experimental data in Fig. 6, and the best fit parameters are listed in the Table S1. The DP7 chains in LiOH aqueous solutions can be described as a rigid slab of thickness ~ 4 Å, width ~ 8 Å, and lengths about 34-42 Å. Using the same slab model with fixed thickness and width

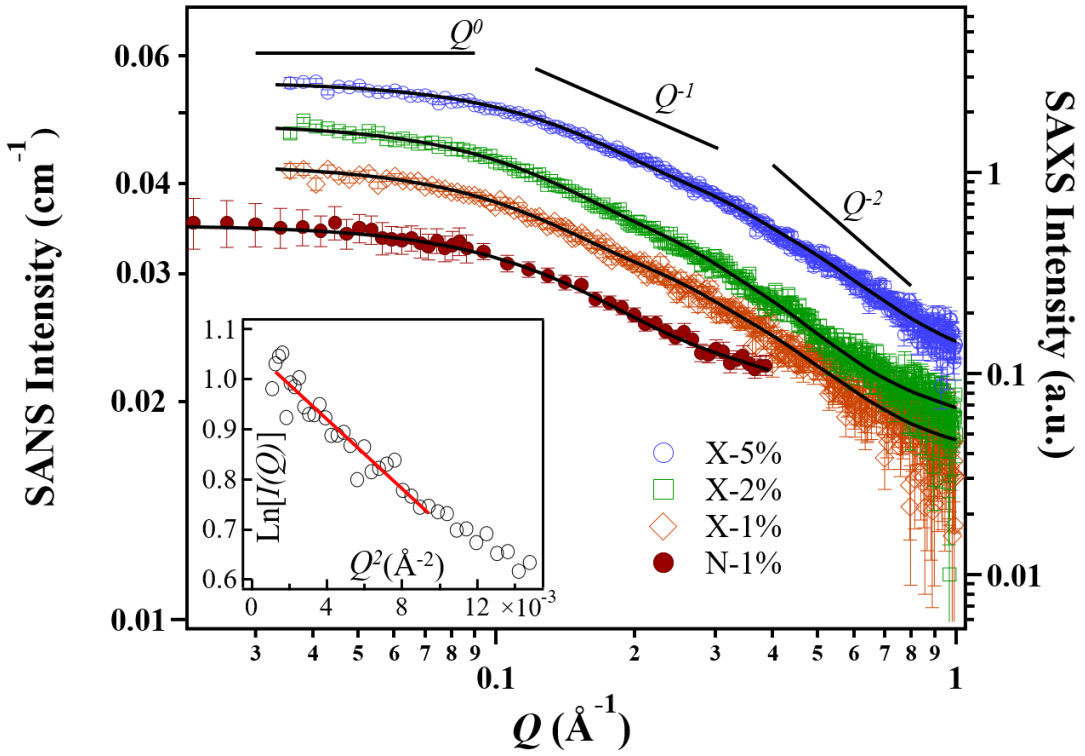

quantities from SAXS, fitting to SANS (curve through the data in Fig. 6) yields L = 29 ± 3 Å, slightly smaller than those from SAXS. The fitted length from SAXS/SANS data corresponds to a DP range of 5.6-8.2, consistent with other measurements.

Fig. 6. Experimental data of SAXS on 1 wt % (X-1%, open diamonds), 2 wt % (X-2%, open squares), and 5 wt % (X-5%, open cycles) DP7 in 4 wt % of LiOH and SANS on 1 wt % DP7 in dDMSO (N-1%, filled circles) are shown as symbols with error bars from counting statistics, and the solid curves through symbols are best model fitting calculation. The inset shows Guinier analysis of the SAXS on the 5 wt % DP7 in alkaline solution.

4. Conclusions

We have revisited the classical method of producing oligocellulose through hydrolysis of microcrystalline cellulose in phosphoric acid at room temperature. The oligocellulose products were overall of high purity but also contained a small fraction of mono-substituted cellulose phosphate possibly from the side-reaction of the hydrolysis process. The overall production yield of oligocellulose was about 50%. The lower DP fraction is composed of cellulose molecules from DP5 to DP12, with DP7 being the most abundant species. The number- and weight-averaged molecular weights as measured from the mass spectra were 1339 g/mol and 1388 g/mol respectively, corresponding to the polydispersity index of 1.04. They form type-II crystals in solid powder, and dissolve in alkaline aqueous solutions and dimethyl sulfoxide. Although small in quantity, mono-phosophorylated oligomers were also detected. SAXS and SANS measurements of the solution agreed with theoretical curves of slab object indicating the extended conformation of cellulose oligomers.

Declaration of Competing Interest

The authors declare no conflict of interest.

Acknowledgements

F. Jiang was financially supported by the National Natural Science Foundation of China (Grant 51603199), China Postdoctoral Science Foundation (Grant 2017M622629), and Anhui Provincial Innovation and Entrepreneurship Support Plan for Overseas Returnees (Grant 2020LCX027). We acknowledge the support of the National Institute of Standards and Technology through award 70NANB12H238 and by providing the neutron research facilities used in this study. This work benefited from the use of the SasView application, originally developed under an NSF award DMR-0520547. SasView contains code developed with funding from the European Union's Horizon 2020 research and innovation program under the SINE2020 project, grant agreement No. 654000. We thank Dr. Yimin Mao of NCNR/NIST for help on SANS experiment and data reduction.

Appendix A. Supplementary material

Supplementary material associated with this article is available.

References

[1] H. Kargarzadeh, M. Mariano, D. Gopakumar, I. Ahmad, S. Thomas, A. Dufresne, J. Huang, N. Lin, Advances in cellulose nanomaterials, Cellulose 25 (2018) 2151-2189.

[2] S. Wang, A. Lu, L.N. Zhang, Recent advances in regenerated cellulose materials, Prog. Polym. Sci. 53 (2016) 169-206.

[3] F. Jiang, Z.K. Wang, Y.L. Qiao, Z.G. Wang, C.B. Tang, A novel architecture toward third-generation thermoplastic elastomers by a grafting strategy, Macromolecules 46 (2013) 4772-4780.

[4] S. Agate, M. Joyce, L. Lucia, L. Pal, Cellulose and nanocellulose-based flexible-hybrid printed electronics and conductive composites-a review, Carbohydr. Polym. 198 (2018) 249-260.

[5] O. Garcia-Valdez, P. Champagne, M.F. Cunningham, Graft modification of natural polysaccharides via reversible deactivation radical polymerization, Prog. Polym. Sci. 76 (2018) 151-173.

[6] J.S. Yang, J.F. Li, Self-assembled cellulose materials for biomedicine: a review, Carbohydr. Polym. 181 (2018) 264-274.

[7] F. Jiang, C.Q. Pan, Y.Q. Zhang, Y.X. Fang, Cellulose graft copolymers toward strong thermoplastic elastomers via RAFT polymerization, Appl. Surf. Sci. 480 (2019) 162-171.

[8] M. Meiland, T. Liebert, T. Heinze, Tailoring the degree of polymerization of low molecular weight cellulose, Macromol. Mater. Eng. 296 (2011) 802-809.

[9] S.I. Mussatto, I.M. Mancilha, Non-digestible oligosaccharides: a review, Carbohydr.

311 Polym. 68 (2007) 587-597.
312 [10] P.R. Chen, A. Shrotri, A. Fukuoka, Soluble cello-oligosaccharides produced by
313 carbon-catalyzed hydrolysis of cellulose, ChemSusChem 12 (2019) 2576-2580.
314 [11] F. Nakatsubo, H. Kamitakahara, M. Hori, Cationic ring-opening polymerization of 3,
315 6-di-*O*-benzyl-*α*-*D*-glucose 1,2,4-orthopivalate and the first chemical synthesis of
316 cellulose, J. Am. Chem. Soc. 118 (1996) 1677-1681.
317 [12] S. Kobayashi, K. Kashiwa, T. Kawasaki, S. Shoda, Novel method for polysaccharide
318 synthesis using an enzyme: the first in vitro synthesis of cellulose via a nonbiosynthetic
319 path utilizing cellulase as catalyst, J. Am. Chem. Soc. 113 (1991) 3079-3084.
320 [13] C.J. Knill, J.F. Kennedy, Degradation of cellulose under alkaline conditions,
321 Carbohydr. Polym. 51 (2003) 281-300.
322 [14] R. Gupta, Y. Lee, Mechanism of cellulase reaction on pure cellulosic substrates,
323 Biotechnol. Bioeng. 102 (2009) 1570-1581.
324 [15] T. Zweckmair, J.T. Oberlerchner, S. Bohmdorfer, M. Bacher, V. Sauerland, T.
325 Rosenau, A. Potthast, Preparation and analytical characterisation of pure fractions of
326 cellooligosaccharides, J. Chromatogr. A 1431 (2016) 47-54.
327 [16] E. Billes, K.N. Onwukamike, V. Coma, S. Grelier, F. Peruch, Cellulose oligomers
328 production and separation for the synthesis of new fully bio-based amphiphilic
329 compounds, Carbohydr. Polym. 154 (2016) 121-128.
330 [17] M. Voloch, M.R. Ladisch, M. Cantarella, G.T. Tsao, Preparation of cellodextrins

using sulfuric acid, Biotechnol. Bioeng. 26 (1984) 557-559.

[18] O. Akpinar, R.J. McGorrin, M.H. Penner, Cellulose-based chromatography for cellooligosaccharide production, J. Agric. Food Chem. 52 (2004) 4144-4148.

[19] T. Liebert, M. Seifert, T. Heinze, Efficient method for the preparation of pure, water-soluble cellodextrines, Macromol. Symp. 262 (2008)140-149.

[20] A. Isogai, M. Usuda, Preparation of low-molecular weight celluloses using phosphoric acid, Mokuzai Gakkaishi 37 (1991) 339-344.

[21] M. Schwanninger, J.C. Rodrigues, H. Pereira, B. Hinterstoisser, Effects of short-time vibratory ball milling on the shape of FT-IR spectra of wood and cellulose, Vib. Spectrosc. 36 (2004) 23-40.

[22] Y. Yataka, T. Sawada, T. Serizawa, Enzymatic synthesis and post-functionalization of two-dimensional crystalline cellulose oligomers with surface-reactive groups, Chem. Commun. 51 (2015) 12525-12528.

[23] Z.H. Liu, X.F. Sun, M.Y. Hao, C.Y. Huang, Z.M. Xue, T.C. Mu, Preparation and characterization of regenerated cellulose from ionic liquid using different methods, Carbohydr. Polym. 117 (2015) 99-105.

[24] C.-H. Kuo, C.-K. Lee, Enhancement of enzymatic saccharification of cellulose by cellulose dissolution pretreatments, Carbohydr. Polym. 77 (2009) 41-46.

[25] M. Adsul, S.K. Soni, S.K. Bhargava, V. Bansal, Facile approach for the dispersion of regenerated cellulose in aqueous system in the form of nanoparticles, Biomacromolecules

351 13 (2012) 2890-2895.
352 [26] S.Y. Oh, D.I. Yoo, Y. Shin, H.C. Kim, H.Y. Kim, Y.S. Chung, W.H. Park, J.H. Youk,
353 Crystalline structure analysis of cellulose treated with sodium hydroxide and carbon
354 dioxide by means of X-ray diffraction and FTIR spectroscopy, Carbohydr. Res. 340 (2005)
355 2376-2391.
356 [27] P. Langan, Y. Nishiyama, H. Chanzy, A revised structure and hydrogen-bonding
357 system in cellulose II from a neutron fiber diffraction analysis, J. Am. Chem. Soc. 121
358 (1999) 9940-9946.
359 [28] P. Langan, Y. Nishiyama, H. Chanzy, X-ray structure of mercerized cellulose II at 1
360 Å resolution, Biomacromolecules 2 (2001) 410-416.
361 [29] L.A. Flugge, J.T. Blank, P.A.J.J.o.t.A.C.S. Petillo, Isolation, modification, and NMR
362 assignments of a series of cellulose oligomers, J. Am. Chem. Soc. 121 (1999) 7228-7238.
363 [30] B. Bernet, A. Vasella, Intra- and intermolecular H-bonds of alcohols in DMSO,
364 ^{1}H-NMR analysis of inter-residue H-bonds in selected oligosaccharides: cellobiose,
365 lactose, *N*,*N*′-diacetylchitobiose, maltose, sucrose, agarose, and hyaluronates, Helv. Chim.
366 Acta 83 (2000) 2055-2071.
367 [31] H. Sugiyama, K. Hisamichi, T. Usui, K. Sakai, J. Ishiyama, A study of the
368 conformation of β-1,4-linked glucose oligomers, cellobiose to cellohexaose, in solution, J.
369 Mol. Struct. 556 (2000) 173-177.
370 [32] J.S. Moulthrop, R.P. Swatloski, G. Moyna, R.D.J.C.c. Rogers, High-resolution ^{13}C

371 NMR studies of cellulose and cellulose oligomers in ionic liquid solutions, Chem.
372 Commun. (2005) 1557-1559.
373 [33] D.M. Petrovic, I. Kok, A.J.J. Woortman, J. Ciric, K. Loos, Characterization of
374 oligocellulose synthesized by reverse phosphorolysis using different cellodextrin
375 phosphorylases, Anal. Chem. 87 (2015) 9639-9646.
376 [34] A. Adharis, D.M. Petrović, I. Özdamar, A.J. Woortman, K. Loos, Environmentally
377 friendly pathways towards the synthesis of vinyl-based oligocelluloses, Carbohydr.
378 Polym. 193 (2018) 196-204.
379 [35] A.R. Horrocks, Textile flammability research since 1980-personal challenges and
380 partial solutions, Polym. Degrad. Stab. 98 (2013) 2813-2824.
381 [36] A. Isogai, R.H. Atalla, Dissolution of cellulose in aqueous NaOH solutions,
382 Cellulose 5 (1998) 309-319.
383 [37] J. Cai, Y.T. Liu, L.N. Zhang, Dilute solution properties of cellulose in LiOH/urea
384 aqueous system, J. Polym. Sci., Part B: Polym. Phys. 44 (2006) 3093-3101.
385 [38] J. Hagman, L. Gentile, C.M. Jessen, M. Behrens, K.E. Bergqvist, U. Olsson, On the
386 dissolution state of cellulose in cold alkali solutions, Cellulose 24 (2017) 2003-2015.
387 [39] X.Y. Jiang, S. Kitamura, T. Sato, K. Terao, Chain dimensions and stiffness of
388 cellulosic and amylosic chains in an ionic liquid: cellulose, amylose, and an amylose
389 carbamate in BmimCl, Macromolecules 50 (2017) 3980-3985.
390 [40] J.P. Zhou, L.N. Zhang, J. Cai, Behavior of cellulose in NaOH/urea aqueous solution

391 characterized by light scattering and viscometry, J. Polym. Sci., Part B: Polym. Phys. 42
392 (2004) 347-353.
393